Mixing layers and coherent structures in vegetated aquatic flows

Marco Ghisalberti and Heidi M. Nepf

Ralph M. Parsons Laboratory, Department of Civil and Environmental Engineering, Massachusetts Institute of Technology, Cambridge, Massachusetts, USA

[1]   To date, flow through submerged aquatic vegetation has largely been viewed as perturbed boundary layer flow, with vegetative drag treated as an extension of bed drag. However, recent studies of terrestrial canopies demonstrate that the flow structure within and just above an unconfined canopy more strongly resembles a mixing layer than a boundary layer. This paper presents laboratory measurements, obtained from a scaled seagrass model, that demonstrate the applicability of the mixing layer analogy to aquatic systems. Specifically, all vertical profiles of mean velocity contained an inflection point, which makes the flow susceptible to Kelvin-Helmholtz instability. This instability leads to the generation of large, coherent vortices within the mixing layer (observed in the model at frequencies between 0.01 and 0.11 Hz), which dominate the vertical transport of momentum through the layer. The downstream advection of these vortices is shown to cause the progressive, coherent waving of aquatic vegetation, known as the monami. When the monami is present, the turbulent vertical transport of momentum is enhanced, with turbulent stresses penetrating an additional 30% of the plant height into the canopy.   INDEX TERMS: 1845 Hydrology: Limnology; 1890 Hydrology: Wetlands; 4211 Oceanography: General: Benthic boundary layers; 4568 Oceanography: Physical: Turbulence, diffusion, and mixing processes; KEYWORDS: vegetated flow, mixing layer, monami, seagrass, vortices, turbulence

1.   Introduction

[2]   By altering the hydrodynamic conditions, submerged aquatic vegetation can dramatically affect the fate and transport of sediment, nutrients, contaminants, dissolved oxygen, and fauna in aquatic systems [*Fonseca and Kenworthy*, 1987; *Nepf*, 1999]. The extent of research into the hydrodynamic effects of aquatic vegetation does not reflect the importance of the topic; however, studies of atmospheric flows through terrestrial vegetation are prevalent [e.g., *Finnigan and Mulhearn*, 1978; *Finnigan*, 1979a, 1979b; *Raupach et al.*, 1996]. While the two situations are analogous, atmospheric flows are essentially unbounded vertically, meaning that the vegetated flow is superimposed upon an atmospheric boundary layer of a much larger scale. Of particular interest for aquatic canopies therefore is the transition from fully bounded flow (emergent vegetation) to virtually unbounded flow (thoroughly submerged vegetation). Note that although not entirely literal, the term "canopy" is used in this paper to describe an assemblage of plants.

[3]   In flows through submerged vegetation, the vertical discontinuity of the drag results in strong velocity shear at the top of the canopy and greatly increased turbulence intensities in this region, relative to unobstructed flow [*Gambi et al.*, 1990; *Vivoni*, 1998; *Wallace et al.*, 1998]. In addition, coherent, canopy-scale eddies have been observed to dominate vertical momentum fluxes into terrestrial [*Raupach and Shaw*, 1982; *Gao et al.*, 1989; *Raupach et al.*, 1996] and aquatic canopies [*Ikeda and Kanazawa*, 1996; *Wallace et al.*, 1998]. By analogy, these eddies should have tremendous implications for scalar fluxes that govern oxygen exchange, seed dispersal, sediment deposition, and chemical reactions in aquatic canopies [*Wallace et al.*, 1998].

[4]   In response to steady currents, submerged aquatic vegetation may exhibit a progressive, synchronous, large-amplitude waving (termed "monami" by *Ackerman and Okubo* [1993])

[*Fonseca and Kenworthy*, 1987; *Grizzle et al.*, 1996]. The monami is triggered when flow velocity increases above a threshold value; this threshold increases as the flow depth is reduced [*Ghisalberti*, 2000]. Several researchers [*Murota et al.*, 1984; *Ackerman and Okubo*, 1993; *Grizzle et al.*, 1996; *Wallace et al.*, 1998] have also identified distinct peaks between 0.1 and 0.6 Hz in spectra of streamwise velocity measured within aquatic canopies. *Ackerman and Okubo* [1993] postulated that the periodic velocity fluctuations are caused by plant waving. This paper, however, presents an argument for the converse causal relationship, namely, that the monami is itself a response to the strong oscillations in streamwise velocity associated with the passage of coherent vortex structures.

[5]   The underlying theme of this paper is demonstration of the analogy between aquatic flows with submerged vegetation and mixing layers, an analogy developed for terrestrial canopies by *Raupach et al.* [1996]. Until that publication, flow within and above terrestrial canopies was regarded as perturbed boundary layer flow. The flow is now understood to be closer to a mixing layer, a free shear layer (i.e., one where the shear does not arise from boundary conditions) characterized by two regions of constant velocity separated by a confined region of shear containing an inflection point (Figure 1). The velocity profile of a mixing layer approximates that of a hyperbolic tangent [*Ho and Huerre*, 1984]. *Raupach et al.* [1996] showed that several characteristics of vegetated terrestrial flows resembled those of a mixing layer, including the inflection point in the velocity profile, the increased correlation between horizontal and vertical turbulent fluctuations, and the structure of momentum transfer.

[6]   Rayleigh proved that a necessary criterion for instability of a parallel flow is that the basic velocity profile has a point of inflection [*Kundu*, 1990, p. 392]. This condition is satisfied by a hyperbolic tangent velocity profile, such that mixing layers are subject to Kelvin-Helmholtz (KH) instability at every stage in their development [*Holmes et al.*, 1996]. This wave instability grows until it billows into roller-type vortices [*Brown and Roshko*, 1974; *Ho and Huerre*, 1984; *Holmes et al.*, 1996], as
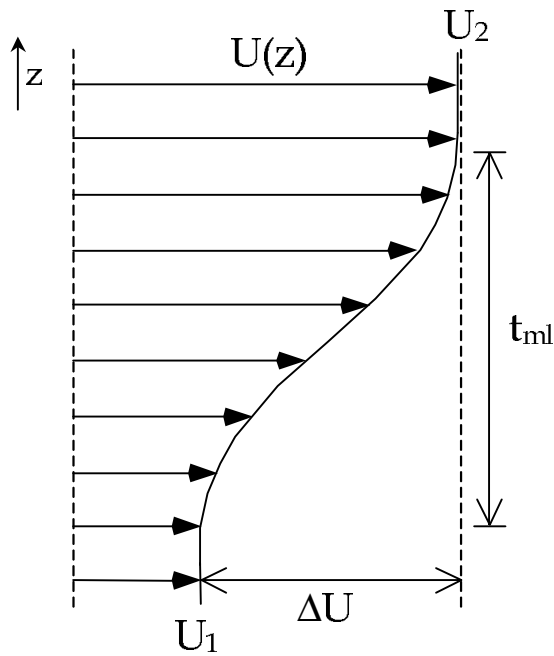
Figure 1. Definitive diagram of mixing layer variables. U is mean velocity; U_1 and U_2 are the low- and high-stream velocities, respectively; $\Delta U = U_2 - U_1$; and t_{ml} is the thickness of the mixing layer defined (nominally) with end points $(U - U_1)/\Delta U = 0.01$ and $(U_2 - U)/\Delta U = 0.01$. The parameter $\bar{z}$ is defined as the height at which $U = \overline{U} = 1/2\,(U_1 + U_2)$.

shown in the gaseous mixing layer of Figure 2. These vortices dominate mass and momentum transfer through the mixing layer [*Ho et al.*, 1991]. The frequency of the KH instability, f_{KH}, is related to the momentum thickness of the mixing layer (θ):

$$f_{\mathrm{KH}} = 0.032\left(\frac{\overline{U}}{\theta}\right) \qquad (1)$$

[*Ho and Huerre*, 1984], where, with reference to Figure 1, $\overline{U}$ is the arithmetic mean of U_1 and U_2 and θ is defined by

$$\theta = \int\limits_{-\infty}^{\infty}\left[\frac{1}{4} - \left(\frac{U - \overline{U}}{\Delta U}\right)^2\right]dz \qquad (2)$$

[*Rogers and Moser*, 1994]. Equation (1) is conceptually reasonable, as the frequency of vortex passage is expected to be proportional to their advection speed and inversely proportional to their size, which is strongly linked to mixing layer thickness.

[7] A comparison between predicted KH frequencies (from (1)) and observed frequencies drawn from the aquatic literature is shown in Figure 3. In each case, $\overline{U}$ and θ were calculated from mean velocity profiles provided and were used to predict f_{KH}. Observed frequencies were based on either the peak in streamwise velocity spectra [*Wallace et al.*, 1998], the frequency of vortex passage observed in flow visualization experiments [*Ikeda and Kanazawa*, 1996], or the observed monami frequency [*Vivoni*, 1998]. In the final case the monami frequencies were obtained from our own analysis of video footage provided by the author (E. Vivoni, Massachusetts Institute of Technology, personal communication, 1999), which corrected for the factor of 2 omitted in his original analysis. The strong agreement between predicted and observed frequencies suggested that peaks in streamwise velocity spectra are associated with the KH instability and that this instability ultimately generates the monami. The experiments detailed in this paper sought to validate this hypothesis through spectral analysis and direct observation of the monami in several flow scenarios.

[8] The goals of the experiment were to use a model seagrass canopy, first, to examine the mixing layer analogy for flow through flexible, submerged aquatic vegetation and, second, to explain the generation of the monami and determine its effect on vertical turbulent exchange between the canopy and the overlying water.

2. Scaling Criteria for Model Vegetation

[9] The model vegetation (subscript m) was designed to satisfy both dynamic and geometric similarity with a prototypical eelgrass (*Zostera marina*) meadow (subscript p). The motion of an eelgrass blade is governed by a drag force (F_D), a buoyancy force (F_B), and a restoring force due to the blade's rigidity (F_R). Dynamic similarity is achieved by matching the two independent ratios of these governing forces. With important geometric parameters of eelgrass blades defined in Figure 4, the internal moment in a bent blade, M_I, is given by

$$M_I = J\frac{\partial^2 x}{\partial z^2}, \qquad (3)$$

where J ($= Ewt^3/12$, E denoting the modulus of elasticity) represents the flexural rigidity of the blade. Therefore

$$F_R \sim \frac{M_I}{h} \sim \frac{J}{h}\left(\frac{l}{h_d^2}\right). \qquad (4)$$
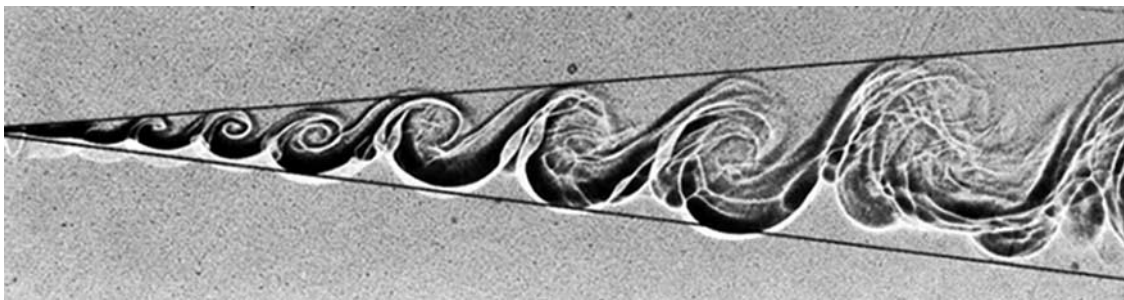

Figure 2. Shadowgraph of a mixing layer between two gaseous streams flowing from left to right. Vortex generation and growth is evident; these vortices dominate mass and momentum transfer through the mixing layer [from *Brown and Roshko*, 1974] (reprinted with the permission of Cambridge University Press).
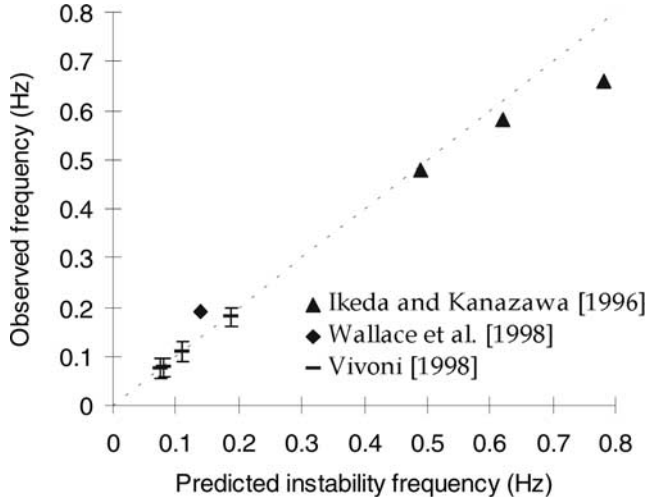
Figure 3. Comparison between observed frequencies and the predicted instability frequencies of mixing layers generated in vegetated aquatic flows. Vertical bars are indicative of uncertainty in the observed frequency. The dashed line represents perfect agreement.

Since $l = h_d \tan \alpha$ ($\approx h \sin \alpha$ for small deflections), (4) becomes

$$F_R \sim \frac{J}{h}\left(\frac{h \sin \alpha}{h^2 \cos^2 \alpha}\right) = \frac{J}{h^2} f_1(\alpha) , \qquad (5)$$

where

$$f_1(\alpha) = \frac{\sin \alpha}{\cos^2 \alpha} .$$

Therefore for small deflections the ratios of the governing forces will have the following scales:

$$\frac{F_B}{F_R} \sim \frac{(\rho_w - \rho_s)ghwt}{(J/h^2)f_1(\alpha)} \sim \frac{(\rho_w - \rho_s)gh^3}{Et^2 f_1(\alpha)} \qquad (6)$$
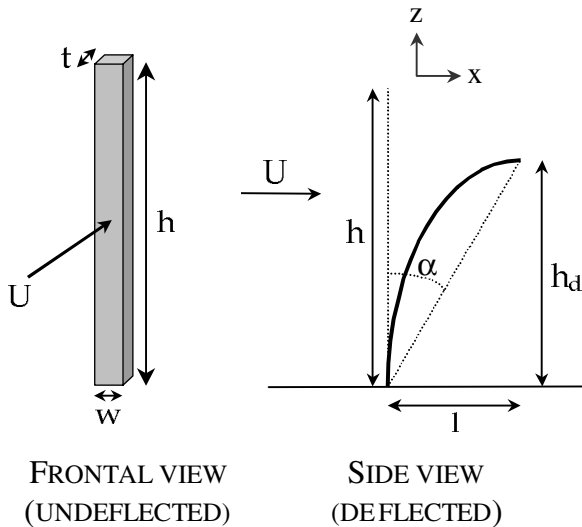
and

$$\frac{F_R}{F_D} \sim \frac{(J/h^2)f_1(\alpha)}{\rho_w \, A_f C_D U_c^2} \sim \frac{Et^3 f_1(\alpha)}{h^3 \cos \alpha \, C_D U_c^2} , \qquad (7)$$

where ρ_w and ρ_s are the densities of water and of the blade, respectively; g is gravitational acceleration; A_f is the frontal area of the blade; U_c is the mean in-canopy velocity; and C_D is the blade drag coefficient. As α describes plant geometry, it is expected that it will have a pronounced effect on flow geometry, so individual experimental flow scenarios only faithfully model a prototypical flow for which $\alpha_m = \alpha_p$. Under this caveat we require that $\cos \alpha_m = \cos \alpha_p$ and $f_1(\alpha_m) = f_1(\alpha_p)$. Additionally, the drag coefficient of a plate aligned normal to the flow displays only a weak dependence on Reynolds number [*Gerhart et al.*, 1992, p. 597]. Therefore, given geometric similarity, C_D can be treated as a constant. By excluding parameters that are approximately equal in the model and in the identically deflected prototype (i.e., g, ρ_w, C_D, $f_1(\alpha)$ and $\cos \alpha$), the dynamic ratios (6) and (7), dimensional after parameter exclusion, become,

$$\lambda_1 = \frac{(\rho_w - \rho_s)h^3}{Et^2} \qquad (8)$$

and

$$\lambda_2 = \frac{Et^3}{h^3 U_c^2} , \qquad (9)$$

respectively. The dependence of λ_2 on U_c^2 makes its value vary tremendously in the field, so λ_1 was chosen as the critical design parameter. However, if $\lambda_{1,m} = \lambda_{1,p}$ and $\alpha_m = \alpha_p$, then λ_2 will automatically be matched between the model and the prototype. Given the uncertainty of several field parameters, the value of $\lambda_{1,p}$ conceivably ranges between 10^{-3} and 10^0 s^2 m^{-1} (for details, see *Ghisalberti* [2000]). Trial plants encompassing a range of values of λ_1 (0.006–0.092 s^2 m^{-1}) were subjected to a wave-current environment. The plant with $\lambda_1 = 0.055$ s^2 m^{-1} exhibited the most realistic behavior, as compared with video

Figure 4. Definition of geometric characteristics of eelgrass blades, including h, the total length of the blade, and h_d, the deflected height of the blade in the flow.
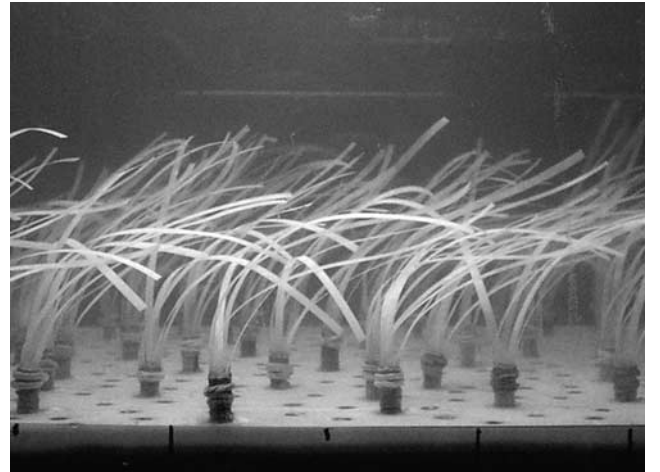

Figure 5. Photograph of the model eelgrass meadow. The meadow comprised 850 randomly placed model plants, each consisting of six thin blades affixed to a wooden stem.
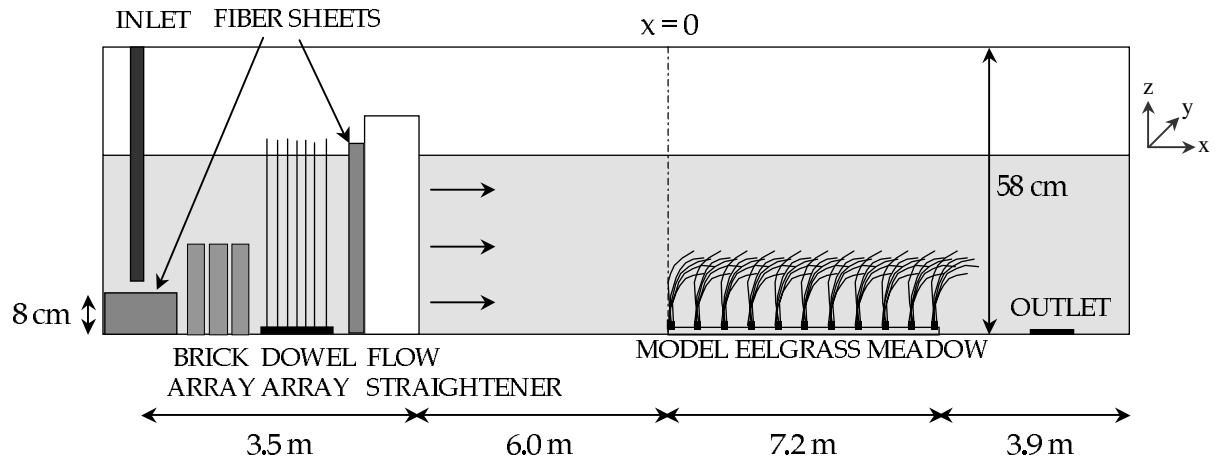
Figure 6. Experimental configuration in the recirculating laboratory flume (note the vertical exaggeration). Several modifications at the inlet created unidirectional, boundary layer flow.

footage of oceanic seagrass meadows (E. Koch, University of Maryland, personal communication, 1998), whose buoyancy and low rigidity create a whip-like motion, dissimilar to the rigid motion of a cantilever.

[10] Additional dimensionless parameters needed to fully describe the flume and canopy conditions include the following:

$$ha, \frac{H}{h}, \frac{p_i}{h} \qquad (10)$$

[*Vivoni*, 1998], where H is the flow depth and p_i represents the set of $\{w,t\}$. The frontal area of plants per unit volume, a (m^{-1}), is defined by $a = mw$, where m is the planting density (blades m^{-2}). Equation of the parameters in (10) between model and prototype necessitated the use of the following model parameters: $h_m = 12.7$ cm, $w_m = 3.0$ mm and $m_m = 1890$ blades m^{-2} (*cf* $h_p = 15-250$ cm, $w_p = 2.5-5.0$ mm, and $m_p = 400-6000$ blades m^{-2}), as detailed by *Ghisalberti* [2000]. Each model eelgrass plant consisted of a stem region and six thin blades (Figure 5), based on the typical morphology of Massachusetts Bay eelgrass [*Chandler et al.*, 1996]. Wooden dowels (0.63 cm in diameter, 2.0 cm in height) were used to mimic the eelgrass stem. Model blades were cut from low-density polyethylene film ($\rho_s = 920$ kg m^{-3}, $E = 3.0 \times 10^8$ Pa) of thickness (t) 0.10 mm such that $\lambda_{1,m} = 0.055$ s^2 m^{-1}. Because of a general absence of ordered arrays in eelgrass meadows [*Fonseca*, 1998] the 850 model plants were placed randomly in holes drilled into six 1.2-m-long, 38-cm-wide Plexiglas boards (total area of 2.7 m^2).

[11] While matching of the blade height Reynolds number, Re_h (= Uh/v, where v is the kinematic viscosity of water), is desirable, it is difficult given the range of flow velocities and blade heights in the field. Using the depth-averaged current, $Re_{h,p}$ varies between 0 and $O(10^5)$; the values of $Re_{h,m}$ (1100−9400) are well within the observed field range. In the model the hydraulic radius Reynolds number of the open channel (Re_{RH} = UR_H/v) ranged between 840 (transitional) and 10,000 (fully turbulent). However, given that the flow is of a mixing layer type, with the large, coherent structures dominating momentum transport, the effects of Re_{RH} (which describes boundary layer flow) were expected to be insignificant. Importantly, the mixing layer structure and associated vortices were observed under all experimental conditions.

3. Experimental Methods

[12] Laboratory experiments were conducted in a 24-m-long, 38-cm-wide, 58-cm-deep recirculating flume. The experimental configuration is shown in Figure 6. For the coordinate system employed, $x = 0$ is located at the front of the model meadow, $y = 0$ is in the lateral center of the flume, and $z = 0$ is at the bottom of the model eelgrass bed. Sheets of rubberized coconut fiber placed under the inlet rapidly dissipated inflow turbulence. An array of bricks immediately downstream of the inlet destroyed the jet structure of the inflow. Surface-piercing dowels and a honeycomb flow straightener eliminated large-scale turbulence and secondary currents. On the basis of vertical profiles of longitudinal velocity

Table 1. Flow and Plant Parameters of the Nine Flow Scenarios

Scenario	H, cm	Q, × 10^{-2} cm^3 s^{-1}	h_d,[a] cm	Observed Monami ?	A_w,[a] cm
A	35.9	111	8.5	Yes	2.9
B	35.9	46	11.3	Yes	1.0
C	35.9	13	12.9	No	⋯
D	29.0	98	6.4	Yes	2.3
E	29.0	40	9.4	Yes	2.8
F	29.0	8	12.7	No	⋯
G	16.4	48	6.2	Yes	1.6
H	16.4	11	9.4	No	⋯
I	12.3	13	9.0	No	⋯

[a] Values are ± 0.2 cm.

Table 2. Mixing Layer Parameters Defining the Mean Velocity Profile in Each Flow Scenario

Scenario	$\overline{U}$, cm s^{-1}	ΔU, cm s^{-1}	t_{ml}, cm	θ, cm	t_{ml}/θ	t_{ml}/h_d	$\overline{z}$, cm	z_v, cm
A	7.12	10.49	32.2	4.51	7.1	3.8	14.1	13.7
B	3.14	5.03	25.5	3.62	7.0	2.3	14.0	14.7
C	0.89	1.66	19.9	2.71	7.3	1.5	13.2	15.8
D	7.40	10.12	25.6	3.74	6.8	4.0	11.7	11.7
E	3.37	4.66	20.0	2.90	6.9	2.1	11.8	13.4
F	0.88	1.51	17.3	2.38	7.3	1.4	12.7	12.7
G	6.96	7.71	13.8	2.00	6.9	2.2	7.8	9.1
H	2.70	2.84	11.2	1.43	7.8	1.2	9.8	9.8
I	3.38	3.68	5.8	0.91	6.4	0.6	7.9	8.8

taken along the model eelgrass meadow, uniform flow conditions (i.e., $\partial U/\partial x = 0$) were observed for $x > 5$ m. Thus $x = 6.5$ m was chosen as an appropriate sampling point, representative of fully developed in-canopy conditions (total canopy length 7.2 m). The differential roughness between the top of the canopy and the glass sidewalls was expected to cause secondary flows in the flume; such flows would obviously not appear in nature. A detailed transect toward the end of the canopy, where these flows should be most pronounced, indicated that lateral flows above the canopy were less than 0.5% of the mean channel velocity [*Ghisalberti*, 2000].

[13] First, for each of nine flow scenarios, velocity records were taken at $x = 6.5$ m over the entire flow depth at heights separated by 1 cm. Each scenario was characterized by the flow depth (H) and flow rate (Q), as detailed in Table 1. Ten-minute velocity records were taken primarily using a three-dimensional acoustic Doppler veloc-imeter (ADV, 25 Hz), with a two-dimensional laser Doppler veloc-imeter (30–100 Hz) used to capture the near-surface region. Directly adjacent to either probe, the removal of up to four plants was required; *Ikeda and Kanazawa* [1996] showed that this removal has no significant effect on the flow. Velocity records were taken at three lateral positions (separated by 3 cm) to capture the stem-scale variability in the flow. The velocity statistics from these three positions were averaged laterally to provide an estimate of the mean, homogenous (in x and y) condition [see, e.g., *Kaimal and Finnigan*, 1994, pp. 84–87]. A temporal and spatial average of the deflected canopy height (h_d) was estimated for all scenarios by measuring the height of 10 model plants during several stages of the monami cycle (if applicable). From video recordings of the canopy at $x = 6.5$ m the monami frequency was calculated by noting the number of waving cycles exhibited by the plants in a 6-min period. The waving amplitude (A_w), estimated from the recordings as the difference between h_d and the minimum instantaneous plant height, was as large as 0.36 h_d, as reported in Table 1.

[14] In a second set of experiments, two ADV probes, separated longitudinally, were used to estimate the velocity (U_v) of the coherent vortices generated in the mixing layer. The separation distance of the probes (between 0.5 and 1.6 m) was sufficiently large to make negligible any error incurred by the manual com-
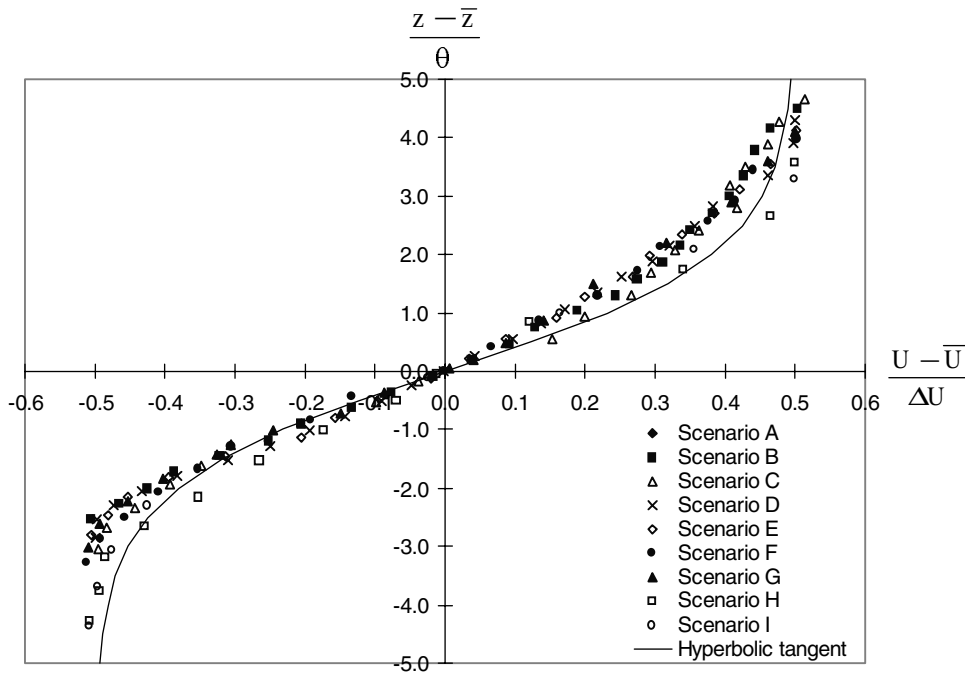

Figure 7. The collapse of the mean velocity profiles for all flow scenarios. The profiles have been shifted by the mean mixing layer velocity and height ($\overline{U}$ and $\overline{z}$) and normalized by ΔU ($= U_2 - U_1$) and the momentum thickness (θ). Note that the top of the canopy lies at $(z - \overline{z})/\theta \approx -0.5$. The comparison between the observed velocity profiles and the hyperbolic tangent profile of a mixing layer is favorable, highlighting the validity of the mixing layer analogy for vegetated aquatic flows.
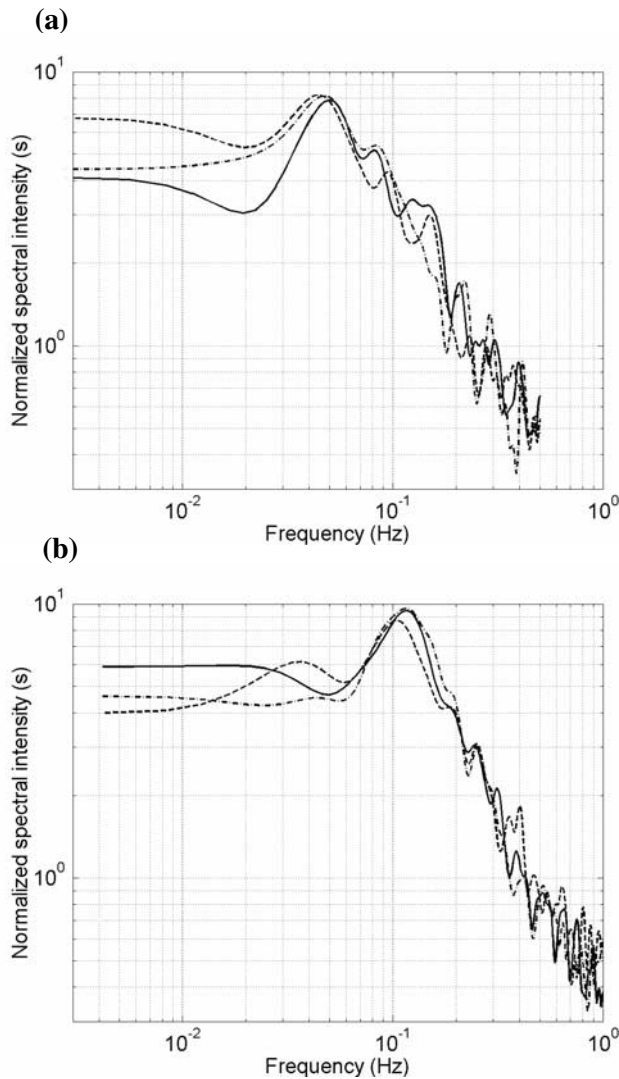
(a)

(b)

Figure 8. Evidence of the prominence and invariance over depth of peaks in spectra of streamwise velocity in and above the model canopy: (a) scenario A ($z/h_d = 1.37$ (solid line), $z/h_d = 0.83$ (dashed line), and $z/h_d = 0.72$ (dashed-dotted line)), $f_r = 1$ Hz, and $w_w = 60$; (b) scenario G ($z/h_d = 0.93$ (solid line), $z/h_d = 1.14$ (dashed line), and $z/h_d = 0.80$ (dashed-dotted line)), $f_r = 2$ Hz, and $w_w = 80$.

mencement of both recordings. Both probes were positioned in the region of uniform flow ($x > 5$ m) so that the momentum thickness remained essentially constant (changing by less than 1%) between the probes; vortex growth and evolution between the probes were thus expected to be small. To estimate vortex velocity, the 10-min streamwise velocity record of the downstream probe was successively lagged against the record of the upstream probe. When the cross-correlation between the two records was maximized, the lag was taken as the time required for an individual vortex to travel between the probes. For each flow scenario, three vortex velocity estimates were obtained.

4. Results

4.1. Mixing Layers in Vegetated Flows

[15] Using the mixing layer analogy for vegetated flows, mixing layer parameters defining the mean velocity profile in

each flow scenario are shown in Table 2. Mean velocity profiles for all flow scenarios contained an inflection point and qualitatively resembled the typical (hyperbolic tangent) profile of a mixing layer, namely,

$$\frac{U - \overline{U}}{\Delta U} = 0.5 \tanh\left(\frac{z - \bar{z}}{2\theta}\right). \tag{11}$$

The profiles are plotted together in Figure 7, with velocity and height axes shifted by $\overline{U}$ and z (respectively) and normalized by ΔU and θ, mixing layer parameters defined in (2) and Figure 1. It is important to note that the mixing layer center, z, lies an average of 0.5 θ above the top of the canopy (h_d). The height of the center of the vortices (z_v in Table 2) was estimated as the height at which w', the turbulent vertical velocity, was maximized. Importantly, the ratio of mixing layer thickness (t_{ml}, defined in Figure 1) to momentum thickness (θ) is similar in all flow scenarios (7.1 ± 0.4). The collapse of the nine experimental velocity profiles (Figure 7) therefore suggests that the profiles of mixing layers generated at the top of submerged aquatic canopies can be estimated with knowledge of just U_1, U_2, t_{ml}, and z.

4.2. Analysis of Velocity Spectra

[16] Velocity spectra were used to examine oscillations in streamwise velocity within the mixing layer for comparison with the predicted vortex frequency, f_{KH}, given by (1). To reduce computation time, records of streamwise velocity were resampled at a frequency (f_r) between 1 and 2 Hz ($\gg f_{KH}$). The autocorrelation functions of the resampled records were then smoothed using a Parzen window with a width (w_w) of between 40 and 80; the spectra were obtained from the smoothed autocorrelation functions. For each flow scenario the frequency of the spectral peak was invariant through the mixing layer (Figure 8). The impact of these strong, periodic velocity oscillations on the canopy is depicted in Figure 9, which shows a time series of streamwise velocity taken at $z/h_d = 0.93$ in scenario G. The velocity record clearly exhibits oscillations of period ~9 s, in agreement with Figure 8b.

[17] The peak frequency in streamwise velocity spectra, the mean monami frequency, and the predicted KH frequency for each flow scenario are shown in Table 3. The strong agreement between these three frequencies confirms that peaks in streamwise velocity spectra are associated with the KH instability and suggests that this instability generates the monami. The frequency of the monami (which dominates plant motion) is considerably lower than the natural frequency of vibration of the vegetation (= 0.6 Hz for the model plants), indicating that the monami is a forced response to the instability of the mixing layer. Spectra of streamwise velocity (e.g., Figure 8) show no evidence of oscillations at 0.6 Hz.

[18] The observations given above and in section 4.1 identify the mechanism of monami generation. When boundary layer flow encounters vegetative drag, the lower lying fluid decelerates, and flow is redirected over the top of the canopy. This leads to the development of a mixing layer profile. Accordingly, the Kelvin-Helmholtz instability develops and rolls over, creating coherent vortices. These vortices are maintained by the shear across the top of the canopy and progress downstream. Therefore plants encounter a stream of vortices and, consequently, an oscillating streamwise velocity, which causes the coherent and progressive waving of the vegetation (Figure 9). In the model, vortex generation appears to occur within the first 0.7 m of the canopy, with coherent waving observed (visually) beyond this point. When the monami is absent (i.e., scenarios C, F, H, and I), spectra of streamwise velocity still exhibit characteristic peaks (Table 3). However, in these cases the kinematics of the vortices
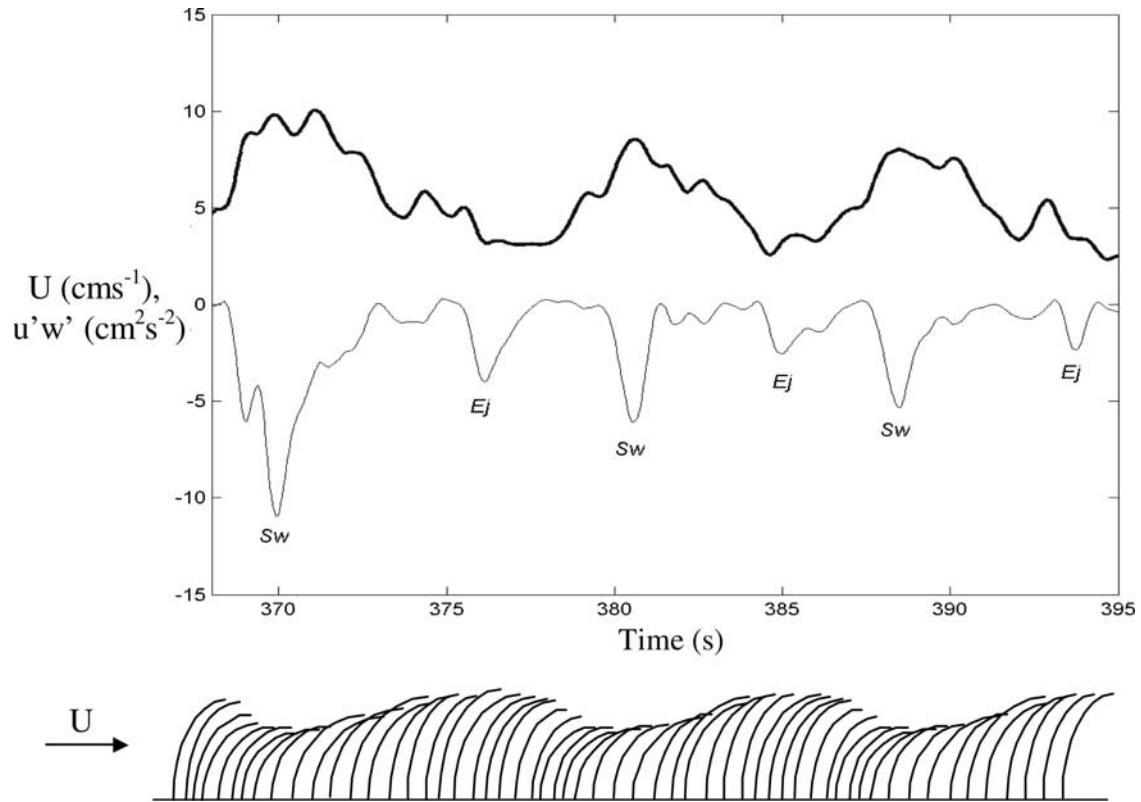
Figure 9. One-second moving averages of strongly oscillatory streamwise velocity (bold line) and Reynolds stress (thin line) records taken at $z/h_d = 0.93$ in scenario G. Strong Reynolds stress events are marked Sw (sweep) ($u' > 0$, $w' < 0$) and Ej (ejection) ($u' < 0$, $w' > 0$). The cartoon depicts the plant response to the flow velocity, which oscillates about a mean of 5.1 cm s^{-1}.

are too weak to cause visible deflections of the plants; this is discussed further in section 4.3.

[19] For all flow scenarios with the monami, three longitudinal "monami channels" were observed, such that the progressive, coherent plant waving within one channel was independent of, and out of phase with, waving in the adjacent channels. This lateral nonuniformity is consistent with observations in terrestrial canopies without artificial lateral boundaries [e.g., *Finnigan*, 2000] and other model aquatic canopies [e.g., *Ikeda and Kanazawa*, 1996]. The three-dimensional nature of the vortices may be explained by a secondary instability that produces streamwise vorticity interwoven

with the primary rollers [*Rogers and Moser*, 1992]. *Finnigan* [2000, Figure 12] presents a conceptual picture of the evolution to a three-dimensional vortex structure of comparable streamwise and lateral dimensions.

4.3. Estimation of Vortex Velocity

[20] Importantly, the monami is visible as the downstream propagation of a localized region of forward plant deflection (Figure 9), indicating the progression of locally enhanced streamwise velocity within the canopy. However, with reference to Figure 1, the mean shear of the mixing layer creates vortices

Table 3. Comparison Between Observed Monami Frequencies, Peak Frequencies in the Spectra of Streamwise Velocity, and the Predicted Frequencies of Mixing Layer Instability

Scenario	Monami Frequency,[a,b] Hz	Peak in Spectra of Streamwise Velocity, Hz	Predicted Mixing Layer Instability Frequency, Hz
A	0.055 ± 0.008	0.052 ± 0.006	0.051 ± 0.002
B	0.028 ± 0.001	0.028 ± 0.003	0.028 ± 0.001
C	⋯	0.012 ± 0.001	0.010 ± 0.001
D	0.064 ± 0.003	0.063 ± 0.007	0.063 ± 0.002
E	0.039 ± 0.005	0.039 ± 0.006	0.037 ± 0.002
F	⋯	0.014 ± 0.002	0.012 ± 0.001
G	0.11 ± 0.01	0.11 ± 0.01	0.11 ± 0.01
H	⋯	0.062 ± 0.006	0.060 ± 0.003
I	⋯	0.11 ± 0.01	0.12 ± 0.01

[a] These values are visual estimates.
[b] Three center dots indicate the absence of the monami in that flow scenario.

Table 4. Estimation of Vortex Velocity Based on the Cross-Correlation of Two Streamwise Velocity Records Taken at Different Locations Along the Canopy

Scenario	Run	U_v, cm s^{-1}	$\overline{U}$,[a] cm s^{-1}	$U_v/\overline{U}$	U_v/U_2
A	1	10.88			
	2	10.19			
	3	9.97			
Average			7.12	1.45 ± 0.07	0.84 ± 0.04
B	1	3.52			
	2	3.55			
	3	3.56			
Average			2.79	1.27 ± 0.01	0.63 ± 0.01
C	1	1.24			
	2	1.17			
	3	1.16			
Average			0.97	1.22 ± 0.04	0.69 ± 0.02
D	1	10.82			
	2	11.22			
	3	10.84			
Average			7.45	1.47 ± 0.03	0.88 ± 0.02
E	1	4.23			
	2	4.29			
	3	4.10			
Average			3.36	1.25 ± 0.03	0.74 ± 0.02
F	1	1.29			
	2	1.25			
	3	1.34			
Average			1.22	1.16 ± 0.03	0.79 ± 0.02
G	1	8.70			
	2	9.26			
	3	9.44			
	4[b]	8.97			
Average			7.12	1.28 ± 0.05	0.84 ± 0.03
H	1	3.21			
	2	3.15			
	3	3.16			
Average			2.69	1.18 ± 0.01	0.77 ± 0.01
I	1	4.47			
	2	4.36			
	3	4.40			
Average			4.03	1.09 ± 0.01	0.84 ± 0.01

[a] Values differ slightly from those in Table 2. These measurements were taken after the completion of the first set of experiments, and the recreation of exactly the same flow conditions was not always possible.

[b] Extra measurement taken because of high variability in the data.

with clockwise circulation. Therefore the passage of a vortex would be expected to contribute a negative perturbation to the velocity field below the vortex center and thus within the canopy (section 4.1). Indeed, in "pure" mixing layers (i.e., those without vegetative drag), vortex circulation can be so pronounced that instantaneous velocity reversal is observed with vortex passage [*Dimotakis et al.*, 1981]. In vegetated flows, however, the passage of a vortex contributes a positive perturbation to the velocity field within the canopy, suggesting that the relative magnitudes of vortex velocity and circulation differ from those in pure mixing layers.

[21] This suggested difference between pure and vegetated mixing layers prompted the study of vortex velocity described in section 3, the results of which are detailed in Table 4. The vortex velocity (U_v) is always greater than the mean mixing layer velocity ($\overline{U}$), in agreement with the flow visualization findings of

Ikeda and Kanazawa [1996] for flow over a submerged canopy. In contrast, $U_v \approx \overline{U}$ in pure mixing layers [*Dimotakis et al.*, 1981; *Ho and Huerre*, 1984; *Panides and Chevray*, 1990]. As expected, the vortex velocity never exceeds the maximum velocity of the mixing layer (U_2). A clear relationship exists between the vortex velocity ratio ($U_v/\overline{U}$) and the mixing layer thickness (t_{ml}), as demonstrated in Figure 10 (where t_{ml} is nondimensionalized by the canopy height, h_d). As the thickness of the mixing layer increases, the vortices become disproportionately affected by the high-stream velocities of the mixing layer, leading to increased velocities of the coherent structures. Although the vortex center (located at z_v, as described in section 4.1) lies slightly above the midpoint of the mixing layer $\left(z_v/\bar{z} = 1.07 \pm 0.08 \right)$, the displacement is insufficient to explain the high vortex velocities, as $U_v > U(z_v)$ in all flow scenarios. Further flow visualization is needed to describe the streamwise mass transport associated with the vortices and will facilitate an explanation for their anomalously high velocity.

[22] In terrestrial canopies the accepted value of U_v is $1.8U_h$ [*Finnigan*, 1979a], where U_h is the mean velocity at the top of the canopy. In this study the mean $\overline{U}/U_h$ ratio is 1.2 (±0.2); assuming a similar ratio for terrestrial vegetation, $U_v/\overline{U} \approx 1.5$ in terrestrial systems. This is consistent with scenarios A and D, which have the most thoroughly submerged vegetation ($H/h_d > 4$). It therefore appears that the value of $U_v/\overline{U}$ asymptotes to ~1.5 as an unconfined canopy condition is approached, concurring with *Vivoni* [1998], who found that t_{ml}/h_d (and thus $U_v/\overline{U}$ from Figure 10), reaches an asymptotic value as H/h_d increases.

[23] The observation of the monami as a downstream progression of forward plant deflection indicates that vortex velocity is sufficiently high that, at the top of the canopy, an increase in streamwise velocity accompanies vortex passage. This is reasonable, considering that U_v is up to 50% greater than $\overline{U}$ (Figure 10), which in turn is greater than U_h, as the top of the canopy (h_d) lies below the mixing layer center (z) in all flow scenarios with the monami. The value of w_{rms} (the standard deviation of the vertical velocity record) at the height of the vortex center (z_v) can be taken as an estimate of the circulation speed within the vortex. The monami is indeed observed when the mean streamwise velocity associated with the vortex ($\approx U_v - w_{rms}|_{z_v}$) is significantly greater than the mean velocity at the top of the canopy. In situations where $\delta U (= U_v - w_{rms}|_{z_v} - U_h)$ is greater than 0.8 cm s^{-1} (i.e., scenarios A, B, D, E, and G), the monami is observed. As shown in Figure 10, this criterion for monami presence (which will vary with vegetation rigidity) is satisfied when $t_{ml}/h_d > 1.5-2.1$. When $\delta U < 0.8$ cm s^{-1}, the vegetation is sufficiently rigid to resist bending during vortex passage, resulting in an absence of the monami.

4.4. Vertical Transport of Momentum Into the Canopy

[24] The efficiency of the turbulent vertical transport of streamwise momentum, r_{uw}, is defined statistically as the correlation coefficient between longitudinal and vertical turbulent fluctuations:

$$r_{uw} = \frac{\overline{u'w'}}{u_{rms}\,w_{rms}}, \qquad (12)$$

where the overbar denotes a temporal average. This parameter can be used to deduce size, location, and strength characteristics of the generated vortices. In boundary layer flow, r_{uw} reaches a maximum (in magnitude) of approximately −0.32. In pure mixing layers this maximum is −0.44, indicative of the strong correlation between u' and w' associated with coherent vortical motion. This demonstrates the importance of the coherent structures in momentum transport and, by implication, scalar fluxes. Furthermore, for flows through terrestrial vegetation, values of r_{uw} reaching −0.5 have been observed [*Raupach*
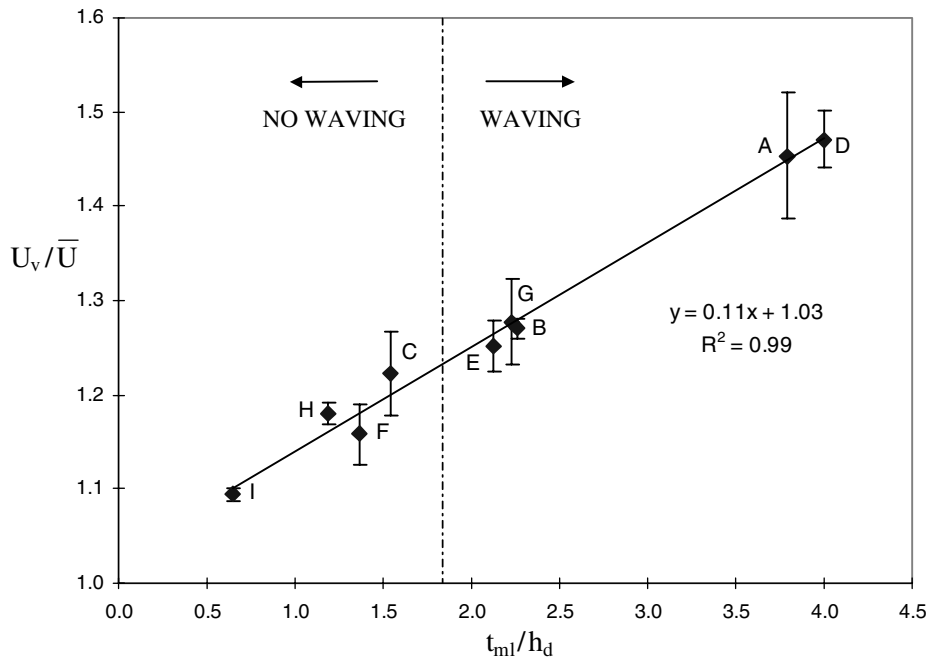
Figure 10. Evidence of the relationship between the vortex velocity ratio ($U_v/\overline{U}$) and (nondimensionalized) mixing layer thickness. As the mixing layer thickness increases, the vortices become disproportionately affected by high-stream velocities and progress at a speed greater than the mean velocity of the mixing layer. Error bars represent 1 standard deviation from the mean. Data point labels indicate the flow scenario in which the measurement was taken.

et al., 1996]. The negative values of r_{uw} in these flows result from the predominance of ejection ($u' < 0$, $w' > 0$) and sweep ($u' > 0$, $w' < 0$) events, causing a downward turbulent transfer of streamwise momentum. Indeed, as observed by *Gao et al.* [1989] and demonstrated in Figure 9, vortex passage creates strong sweeps into the canopy.

[25] Figure 11 shows the vertical profile of r_{uw} for all flow scenarios; the depth of penetration of Reynolds stress $\left(\overline{u'w'}\right)$ into the canopy, h_{uw}, is indicated. In all cases the magnitude of r_{uw} reaches a maximum at the height where shear is maximized (i.e., just below the top of the canopy). For the scenarios with a coherently waving canopy this maximum is approximately -0.5 (Figure 11a) in accordance with the terrestrial canopy observations of *Raupach et al.* [1996]. The decrease of $|r_{uw}|$ is much more rapid below $z = h_d$ than above it, highlighting the inability of the vortices to penetrate into the canopy because of the vegetative drag. Comparison of Figures 11a and 11b demonstrates that when the plants are waving, however, there is a considerably greater penetration of Reynolds stress (associated with the vortices) into the canopy; under waving conditions, $h_{uw} \approx 0.75\ h_d$, whereas, in the absence of waving, $h_{uw} \approx 0.45\ h_d$. This may be explained by the fact that the drag exerted by stationary blades is comparatively greater than that exerted by blades that deflect under strong sweep events. Preliminary laboratory studies suggest that the drag coefficient in the upper 45% of a nonwaving canopy is 3–4 times greater than that in the upper 45% of a waving canopy (M. Ghisalberti, unpublished data, 2001). Consequently, the structure of a vortex is more effectively broken up by nonwaving vegetation, diminishing Reynolds stress penetration. Thus the monami is more than just a passive reflection of momentum transfer into the canopy. A feedback exists between the two, whereby the coherent waving of a canopy strongly enhances vertical transport therein. In all cases, the efficiency of momentum transfer within the mixing layer remains considerably larger than that in unobstructed flow because of the coherent structures that develop.

4.5. Summary of Vortex Mechanics in Vegetated Flows

[26] A schematic diagram summarizing vortex characteristics in vegetated flows is shown in Figure 12. After the Kelvin-Helmholtz instability billows and forms vortices, the structures grow by entrainment of surrounding fluid, thus mixing momentum over greater distances and causing mixing layer growth. The vortices are approximately elliptical in cross section [*Ikeda and Kanazawa*, 1996]. Under the nominal definition that the vertical dimension of the vortices (δ_v) corresponds to the region in which $|r_{uw}| > 0.32$ (the maximum boundary layer value), $\delta_v \approx 6\theta$, which equates roughly with mixing layer thickness, t_{ml} (Table 2). Streamwise vortex spacing (Γ), estimated from $\Gamma = U_v/f_{KH}$, is equal to 6.6 (± 0.7) δ_v. Finally, z_v and $\bar{z}$ increase with distance along the canopy, symptomatic of the gradual redirection of flow over the vegetation.

5. Further Discussion

[27] The presence of the free surface in vegetated aquatic flows implies that frequently, the mixing layer is not literally a free shear layer. Interestingly, when the free surface restricts further mixing layer growth (i.e., when $H - t_{ml} \leq 4$ cm, such as in scenarios A, D, and G), the monami frequency is still in agreement with (1), a relationship derived for free shear layers. Thus the observed vortex frequency is a kinematic property that depends solely on vortex motion and size and is independent of mixing layer evolution.

[28] In contrast to the aquatic canopy studied here, there is poor agreement between linear instability theory and the observed vortex frequency in terrestrial canopies. Several high-Reynolds-number processes may cause this discrepancy, including the emergence of instability modes (due to nonlinearities) other than the fastest growing mode as predicted by linear analysis [*Raupach et al.*, 1996]. The maximum values of Re_h in our model and in prototypical aquatic vegetation are $O(10^4)$ and $O(10^5)$, respec-
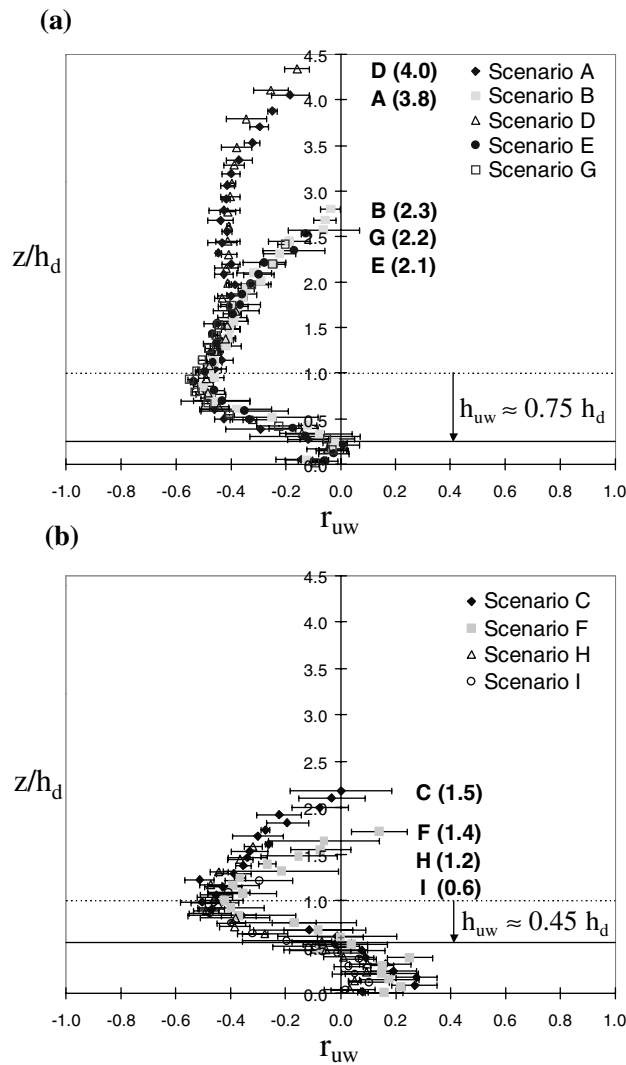
(a)

(b)

Figure 11. Vertical profiles of r_{uw} for flow scenarios (a) with the monami and (b) without the monami. Horizontal bars indicate 1 standard deviation from the lateral mean. The dotted line represents the top of the canopy, and the solid line shows the extent of Reynolds stress penetration into the canopy. Data labels indicate the t_{ml}/h_d ratio for each flow scenario.

[29] The goal of this paper is to provide an understanding of how submerged aquatic vegetation can affect water quality by altering local hydrodynamic conditions. However, because of inherent differences in the turbulent transport of momentum and scalars, analysis of momentum transport merely provides an insight into scalar transport. For example, the transition of mixing layers from laminar to turbulent greatly increases the amount of small-scale scalar mixing, while the effects on momentum transport and mixing layer growth are far less pronounced [*Moser and Rogers*, 1991]. Therefore quantifying scalar fluxes in and above the model canopy, with particular attention paid to comparison with pure mixing layers, is an area of research that requires attention. It is vital in such a study that the generated mixing layers be turbulent; the mixing layer Reynolds number, Re_{ml} (= $\Delta U t_{ml}/\nu$), observed in the field by *Grizzle et al.* [1996] was 2×10^5, much greater than the upper bound of the mixing transition ($\approx 1.7 \times 10^4$ [*Koochesfahani and Dimotakis*, 1986]).

6. Conclusion

[30] Like vegetated terrestrial flows, aquatic flows with submerged vegetation can be patterned on a mixing layer rather than a boundary layer. The vertical discontinuity of the drag creates an inflectional velocity profile, which resembles the hyperbolic tangent profile of a pure mixing layer. The inflectional profile results in the development of a vortex street of Kelvin-Helmholtz instabilities. The downstream progression of these vortices causes strong, periodic oscillations in streamwise velocity, the frequency of which is invariant through the mixing layer. Vortex velocity, greater than the mean velocity of the mixing layer, is sufficient to cause an instantaneous velocity increase at the top of the canopy as a vortex passes. This can, in turn, create localized regions of forward plant deflection that progress smoothly along the canopy; this is the coherent waving phenomenon known as the monami.

[31] Through the action of the coherent vortex structures the vertical transport of streamwise momentum in the generated mixing layers is more efficient than in boundary layers. The vortices dominate the vertical transport of momentum and, by implication, vertical scalar fluxes in the flow. Coherent waving strongly enhances the vertical transport of momentum into the canopy, indicating that the monami is more than just a passive reflection of the flow structure.

tively; Re_h for terrestrial vegetation, however, can reach $O(10^6 - 10^7)$. Therefore it is reasonable to assume that such high-Reynolds-number processes are not occurring in vegetated aquatic flows and certainly not in our scaled model.
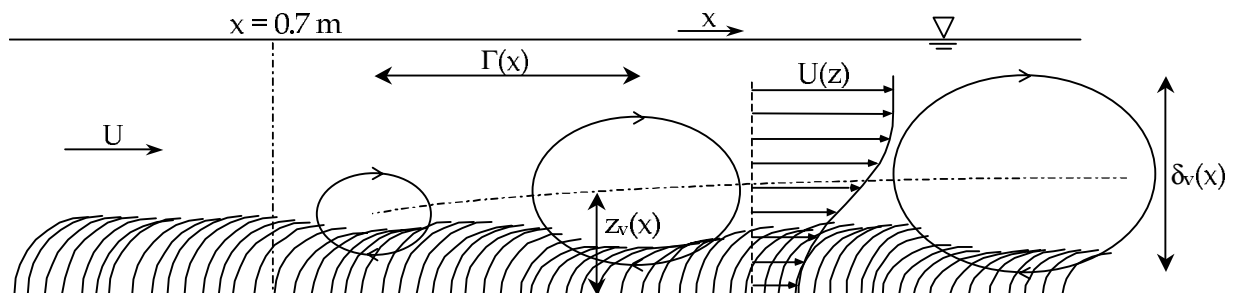

Figure 12. Schematic diagram (exaggerated vertically) of vortex characteristics in vegetated flows. The value of z_v increases with x because of the redirection of flow over the top of the canopy. The monami is observed as the downstream progression of localized areas of forward plant deflection as a result of high vortex velocities.

References

Ackerman, J. D., and A. Okubo, Reduced mixing in a marine macrophyte canopy, *Functional Ecol.*, 7, 305–309, 1993.

Brown, G. L., and A. Roshko, On density effects and large structure in turbulent mixing layers, *J. Fluid Mech.*, 64, 775–816, 1974.

Chandler, M., P. Colarusso, and R. Buchsbaum, A study of eelgrass beds in Boston Harbor and northern Massachusetts bays, report, U.S. Environ. Prot. Agency, Narragansett, R. I., 1996.

Dimotakis, P. E., F. D. Debussy, and M. M. Koochesfahani, Particle streak velocity field measurements in a two-dimensional mixing layer, *Phys. Fluids*, 24(6), 995–999, 1981.

Finnigan, J. J., Turbulence in waving wheat, I, Mean statistics and honami, *Boundary Layer Meteorol.*, 16, 181–211, 1979a.

Finnigan, J. J., Turbulence in waving wheat, II, Structure of momentum transfer, *Boundary Layer Meteorol.*, 16, 213–236, 1979b.

Finnigan, J. J., Turbulence in plant canopies, *Annu. Rev. Fluid Mech.*, 32, 519–571, 2000.

Finnigan, J. J., and P. J. Mulhearn, Modelling waving crops in a wind tunnel, *Boundary Layer Meteorol.*, 14, 253–277, 1978.

Fonseca, M. S., Exploring the basis of pattern expression in seagrass landscapes, Ph.D. thesis, Univ. of Calif., Berkeley, 1998.

Fonseca, M. S., and W. J. Kenworthy, Effects of current on photosynthesis and distribution of seagrasses, *Aquat. Bot.*, 27, 59–78, 1987.

Gambi, M. C., A. R. M. Nowell, and P. A. Jumars, Flume observations on flow dynamics in *Zostera marina* (eelgrass) beds, *Mar. Ecol. Prog. Ser.*, 61, 159–169, 1990.

Gao, W., R. H. Shaw, and K. T. Paw U, Observation of organized structure in turbulent flow within and above a forest canopy, *Boundary Layer Meteorol.*, 47, 349–377, 1989.

Gerhart, P. M., R. J. Gross, and J. I. Hochstein, *Fundamentals of Fluid Mechanics*, 2nd ed., Addison-Wesley-Longman, Reading, Mass., 1992.

Ghisalberti, M., Coherent structures and mixing layers in vegetated aquatic flows, M.S. thesis, Mass. Inst. of Technol., Cambridge, 2000.

Grizzle, R. E., F. T. Short, C. R. Newell, H. Hoven, and L. Kindblom, Hydrodynamically induced synchronous waving of seagrasses: "*monami*" and its possible effects on larval mussel settlement, *J. Exp. Mar. Biol. Ecol.*, 206, 165–177, 1996.

Ho, C.-M., and P. Huerre, Perturbed free shear layers, *Annu. Rev. Fluid Mech.*, 16, 365–424, 1984.

Ho, C.-M., Y. Zohar, J. K. Foss, and J. C. Buell, Phase decorrelation of coherent structures in a free shear layer, *J. Fluid Mech.*, 230, 319–337, 1991.

Holmes, P., J. L. Lumley, and G. Berkooz, *Turbulence, Coherent Structures, Dynamical Systems and Symmetry*, Cambridge Univ. Press, New York, 1996.

Ikeda, S., and M. Kanazawa, Three-dimensional organized vortices above flexible water plants, *J. Hydraul. Eng.*, 122(11), 634–640, 1996.

Kaimal, J. C., and J. J. Finnigan, *Atmospheric Boundary Layer Flows*, Oxford Univ. Press, New York, 1994.

Koochesfahani, M. M., and P. E. Dimotakis, Mixing and chemical reactions in a turbulent liquid mixing layer, *J. Fluid Mech.*, 170, 83–112, 1986.

Kundu, P. K., *Fluid Mechanics*, Academic, San Diego, Calif., 1990.

Moser, R. D., and M. M. Rogers, Mixing transition and the cascade to small scales in a plane mixing layer, *Phys. Fluids A.*, 3(5), 1128–1134, 1991.

Murota, A., T. Fukuhara, and M. Sato, Turbulence structure in vegetated open channel flows, *J. Hydrosci. Hydraul. Eng.*, 2(1), 47–61, 1984.

Nepf, H. M., Drag, turbulence, and diffusion in flow through emergent vegetation, *Water Resour. Res.*, 35(2), 479–489, 1999.

Panides, E., and R. Chevray, Vortex dynamics in a plane, moderate-Reynolds-number shear layer, *J. Fluid Mech.*, 214, 411–435, 1990.

Raupach, M. R., and R. H. Shaw, Averaging procedures for flow within vegetation canopies, *Boundary Layer Meteorol.*, 22, 79–90, 1982.

Raupach, M. R., J. J. Finnigan, and Y. Brunet, Coherent eddies and turbulence in vegetation canopies: The mixing layer analogy, *Boundary Layer Meteorol.*, 78, 351–382, 1996.

Rogers, M. M., and R. D. Moser, The three-dimensional evolution of a plane mixing layer: The Kelvin-Helmholtz rollup, *J. Fluid Mech.*, 243, 183–226, 1992.

Rogers, M. M., and R. D. Moser, Direct simulation of a self-similar turbulent mixing layer, *Phys. Fluids A*, 6(2), 903–923, 1994.

Vivoni, E. R., Turbulence structure of a model seagrass meadow, M.S. thesis, Mass. Inst. of Technol., Cambridge, 1998.

Wallace, S., D. Luketina, and R. Cox, Large scale turbulence in seagrass canopies, paper presented at 13th Australasian Fluid Mechanics Conference, Monash Univ., Melbourne, Victoria, Australia, 1998.

————————

M. Ghisalberti, and H. Nepf, Ralph M. Parsons Laboratory, Department of Civil and Environmental Engineering, Massachusetts Institute of Technology, Cambridge, MA 02139. (marcog@mit.edu; hmnepf@mit.edu)